Analysis of a Droop-Based Power Controller for Three-Phase Microgrids

Andrea Lauri, Hossein Abedini, Davide Biadene, Tommaso Caldognetto, Paolo Mattavelli
University of Padova
Stradella San Nicola, 3
Vicenza, Italy
Email: name.surname@unipd.it

Acknowledgements

This work was supported in part by the project ADPE funded by the Department of Management and Engineering (DTG), University of Padova, Vicenza, Italy, and in part by the research project "Interdisciplinary Strategy for the Development of Advanced Mechatronics Technologies (SISTEMA)", DTG, University of Padova - Project code CUP-C36C18000400001.

Keywords

≪Grid-connected inverter≫, ≪grid-forming converter≫, ≪parallel operation≫,≪seamless transfer≫.

Abstract

A droop-based controller for three-phase converters is described herein. It allows independent control of the converter power at each phase and smooth transitions to the islanded operation. Both three-phase four-wire and three-phase three-wire connections are considered, with a particular focus on the latter configuration. The islanded condition is detected automatically, without the need of communication with other units, and the transition toward the islanded operation mode is performed without interruptions of supply for the energized loads and resources. The considered application scenario is the one of smart microgrids, where power control flexibility and islanded capabilities are features of paramount importance to provide demand-response and uninterrupted operation. A systematic analysis of the approach is presented and validated herein.

Introduction

Low-voltage microgrids provide by means of distributed electronic power converters (EPC) advanced services to the users and upstream grids and continuity of service during emergencies [1]. Examples of crucial features are *i*) uninterrupted supply via islanded operation in response to adverse localized events affecting mainstream electricity supply, *ii*) participation to transactive energy markets [2] by exploiting flexible power flow control, and *iii*) improved power quality in terms of power factor and balanced power absorption [3].

The many requirements are commonly accommodated by means of control hierarchies in which the *P-f* droop control constitutes the primary layer [4], as displayed in Fig. 1. The advantages of droop control include grid voltage support and the capability of adapting the voltage references of EPCs to automatically share the power needs in islanded grids [5]. On the other hand, provisions are necessary to achieve the capability of tracking set-points of output power, which is required for power flow control and for providing services like demand-response.

Then, two opposite needs are present: *i*) support the grid voltage by adapting the inverter output power according to the droop laws, useful especially during islanded operation, *ii*) make the output power fixed and independent from grid voltages and loading conditions to allow power tracking. Remarkably, *P-f*

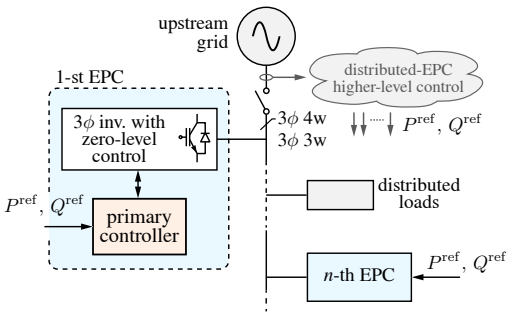

Fig. 1: Application scenario.

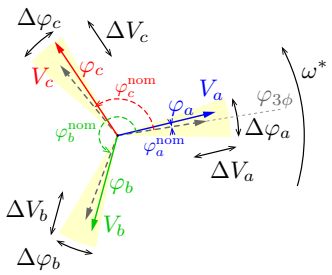

Fig. 2: Quantities involved in Fig. 3-Fig. 4.

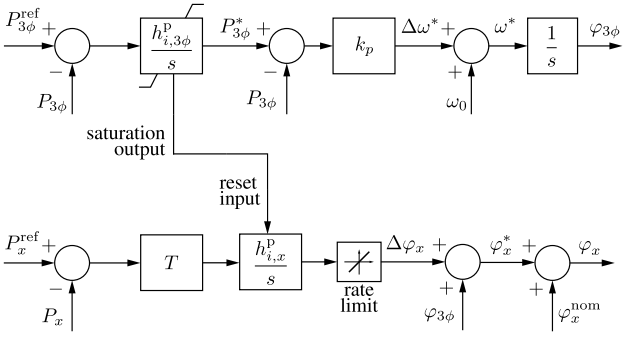

Fig. 3: Proposed primary controller for P-control.

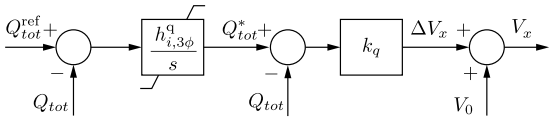

Fig. 4: Proposed primary controller for Q-control.

Table I: Comparison with other approaches

Control kind	**islanded operation**	**grid-tied / islanded transitions**	**three-phase power-tracking**	**per-phase power tracking**
Grid-feeding	-	-	+	+
Traditional droop	+	+	-	-
Droop with 3ϕ P&Q track	+	+	+	-
Approach analyzed herein	+	+	+	+

droop control does not allow *independent* output power control of *each* of the phases of a three-phase converter because it would lead to different frequencies among the phases, which is not acceptable. However, independent power control of each phase is necessary in several circumstances (see, for example, [6, 7, 8, 3, 9, 10, 11]).

A control scheme addressing the three needs discussed above, namely, *i*) control of total output power, *ii*) independent power tracking at converter phases, *iii*) seamless transition toward islanded operation, is proposed and analyzed herein for both three-phase with neutral connection (3ϕ-4w) and *three-phase without neutral* (3ϕ-3w) connection, *iv*) parallel islanded operation with other converters. The challenge of jointly providing all the above features was tacked in [12] considering three-phase four-wire connections to the grid, while the case of absence of the neutral wire, which imposes additional constraints and considerations for the implementation of the control, is discussed herein.

The proposed control scheme is useful in microgrid applications of generic network structures, that is, with or without the availability of the neutral connection. The involved quantities and control scheme are shown in Fig. 2-Fig. 4 and briefly outlined in the following. A comparison with other representative approaches is given in Table I, to highlight the features of this solution as compared to other methods currently available in the literature. Grid-feeding converters, for example, require the presence of the main grid or the presence of other voltage-forming units in order to operate in an islanded microgrid [13]. In traditional droop control, where droop laws are defined as

$$\begin{cases} \omega = \omega_0 - k_p P \\ V = V_0 - k_q Q \end{cases} \tag{1}$$

island operation is possible, however total active and reactive power regulation during grid-tied operation is achievable by modifying the droop laws as in [4] and [14]. In this case of droop with 3ϕ active and reactive power tracking, however, per-phase power regulation is left unexplored. In fact, it is not possible to independently impose droop laws on each phase: this would lead to different frequencies for each phase of the three-phase system.

Of course, a number of other relevant contributions are present in the literature falling within the control kinds referred to in Table I, of which only a few representative papers are mentioned in the brief discussion above.

Basics of Per-Phase Power Control for 3ϕ Networks with Neutral Connection

Per-phase control considering the case of 3ϕ-4w connection is first reviewed next. Operation without the neutral connection (i.e., 3ϕ-3w) is then analyzed in the subsequent section.

The controller is composed of a synchronization loop, displayed in Fig. 3-top, that aligns the instantaneous phase $\varphi_{3\phi}$ of the three-phase inverter voltage to the one of the grid voltage, producing a suitable phase-shift based on the total active power reference signal. Then, the active and reactive power of each phase is regulated by *independent* controllers, in Fig. 3-bottom and Fig. 4. Active power control regulation at each converter phase is achieved by adjusting the phase displacement $\Delta\varphi_x$ of the considered x-th phase with respect to the three-phase $\varphi_{3\phi}$. In order for the regulator in Fig. 3-bottom to process exclusively the differential power (e.g., for phase-a, $P_a - \sum P_x/3$), matrix T is employed, defined as

$$T \triangleq \begin{bmatrix} 2/3 & -1/3 & -1/3 \\ -1/3 & 2/3 & -1/3 \\ -1/3 & -1/3 & 2/3 \end{bmatrix} \tag{2}$$

and consequently the common-mode power (i.e., $\sum P_x/3$) is controlled only by the regulator in Fig. 3-top. This allows to independently set the common mode and differential mode power control bandwidth. Reactive power control is achieved by regulating the amplitude of the generated phase voltages, which can be done phase-by-phase in the case of 3ϕ-4w. To ensure the balance between generated and absorbed power, power control is no longer possible when the system is operating in island conditions: converters must supply the power absorbed by loads connected to the grid. This situation gradually leads to the saturation of the active and reactive control loops, smoothly changing the control structure to grid-forming traditional *P-f* droop structure.

For the sake of clearness, it is worth noticing that by this control scheme active and reactive power control are achieved via phase and amplitude regulation, respectively, which relies on mainly inductive interconnection impedances among the converter and the outer sources. This is a common condition that can be conveniently imposed by a proper zero-level inverter control design.

Per-Phase Power Control for 3ϕ Networks *without* Neutral Connection

Let us consider the power exchange of a single-phase inverter connected to the grid. Be $V_i\angle\varphi_i$ the inverter voltage phasor, and V_g the grid voltage phasor. Considering Thevenin's model of the inverter, namely a voltage generator with a series impedance, connected to the grid, the equations for active and reactive power exchange can be derived. Assuming $\omega = 2\pi f$ the grid frequency, mainly-inductive interconnection impedances, and small voltage and phase differences, the following linearized equations yield [15, 16]:

$$P \simeq \gamma_p \varphi_i\,, \quad Q \simeq \gamma_q\,(V_i - V_g)\,, \qquad \text{with} \quad \gamma_p \triangleq \frac{V_g^2}{\omega L},\ \gamma_q \triangleq \frac{V_g}{\omega L} \tag{3}$$

Such relations hold independently for each of the phases of a 3ϕ-with-N connection. In this case, there is no interdependence between the phases, that is, the power exchange at one phase does not affect the power exchange of the other phases. This is not the case in 3ϕ-without-N connection, which is originally analyzed herein for the controller in Fig. 3 and Fig. 4.

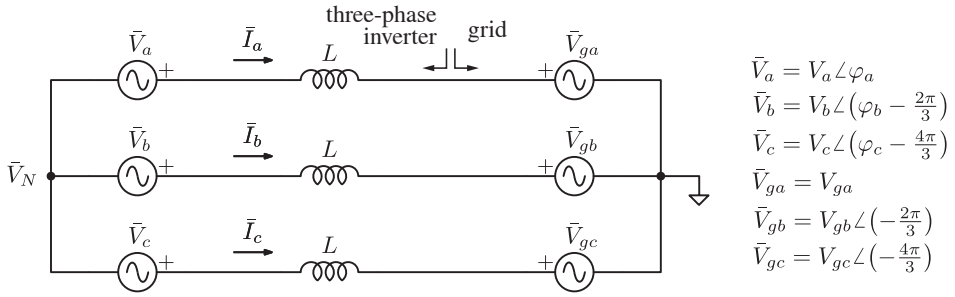

Fig. 5: Thevenin model of a grid-connected three-wires three-phase voltage inverter.

Consider the 3ϕ-without-N connection of Fig. 5 with the indicated nomenclature for voltage phasors. In this case, full independent power control is not physically possible. That is, the power exchanged by one generator is affected by the phase and voltage differences imposed by the others, because the neutral point voltage results $\bar{V}_N = -\left(\bar{V}_a + \bar{V}_b + \bar{V}_c\right)/3$—under the hypothesis of a symmetric grid voltage.

By exploiting the linearized power exchange equations from the Thevenin's model (3), the following matrix representation can be achieved:

$$\begin{bmatrix} P_a \\ P_b \\ P_c \\ Q_a \\ Q_b \\ Q_c \end{bmatrix} = \underbrace{\frac{1}{6}\begin{bmatrix} 4\gamma_p & \gamma_p & \gamma_p & 0 & \sqrt{3}\gamma_q & -\sqrt{3}\gamma_q \\ \gamma_p & 4\gamma_p & \gamma_p & -\sqrt{3}\gamma_q & 0 & \sqrt{3}\gamma_q \\ \gamma_p & \gamma_p & 4\gamma_p & \sqrt{3}\gamma_q & -\sqrt{3}\gamma_q & 0 \\ 0 & -\sqrt{3}\gamma_p & \sqrt{3}\gamma_p & 4\gamma_q & \gamma_q & \gamma_q \\ \sqrt{3}\gamma_p & 0 & -\sqrt{3}\gamma_p & \gamma_q & 4\gamma_q & \gamma_q \\ -\sqrt{3}\gamma_p & \sqrt{3}\gamma_p & 0 & \gamma_q & \gamma_q & 4\gamma_q \end{bmatrix}}_{M} \cdot \begin{bmatrix} \varphi_a \\ \varphi_b \\ \varphi_c \\ \Delta V_a \\ \Delta V_b \\ \Delta V_c \end{bmatrix} \tag{4}$$

where $\Delta V_x = V_x - V_{gx}$. It can be shown that the rank of $M \in \mathbb{R}^{6\times 6}$ is 4, meaning that only four variables can be arbitrarily regulated, while the total six active and reactive powers for phases a, b, and c can not. A possibile choice may be the control of P_a, P_b, Q_a, Q_b, or the control of P_a, P_b, P_c, $Q_{3\phi} = \sum Q_x$. Let us consider the latter option. Then, control of P_a, P_b, P_c, $Q_{3\phi}$ can be achieved with a single voltage amplitude reference signal, the same for all the three-phases of the inverter:

$$\begin{bmatrix} P_a \\ P_b \\ P_c \\ Q_{3\varphi} \end{bmatrix} = \frac{1}{6}\begin{bmatrix} 4\gamma_p & \gamma_p & \gamma_p & 0 \\ \gamma_p & 4\gamma_p & \gamma_p & 0 \\ \gamma_p & \gamma_p & 4\gamma_p & 0 \\ 0 & 0 & 0 & 18\gamma_q \end{bmatrix} \cdot \begin{bmatrix} \varphi_a \\ \varphi_b \\ \varphi_c \\ \Delta V \end{bmatrix} \tag{5}$$

Analysis and Design of the Controller for the 3ϕ-without-N Connection

The proposed controller can be analyzed by deriving its state-space representation in the form:

$$\begin{cases} \dot{x} = Ax + Bu \\ y = Cx + Du \end{cases} \tag{6}$$

which allows design and additional analyses (e.g., stability analysis, state-in-mode participation factors analysis, etc.). Let state vector $x = \left[\varphi_{3\varphi}, \Delta\varphi_a, \Delta\varphi_b, \Delta\varphi_c, P^*_{3\varphi}, Q^*_{3\varphi}\right]^T$, output vector $y = [P_a, P_b, P_c, Q_a, Q_b, Q_c]^T$ and input vector $u = \left[P_a^{ref}, P_b^{ref}, P_c^{ref}, Q_{3\varphi}^{ref}\right]^T$.

Parameter		Value	
P-f droop coefficient	k_p	0.2094	mHz/W
3-phase P saturation limit	$\pm P^{*\text{sat}}_{3\varphi}$	± 6	kW
$Q-V$ droop coefficient	k_q	0.9167	mV/VAr
3-phase Q saturation limit	$\pm Q^{*\text{sat}}_{3\varphi}$	± 6	kVAr
3-phase P contr. integ. gain	$h^{\text{p}}_{i,3\varphi}$	4.3566	1/s
per-phase P contr. integ. gain	$h^{\text{p}}_{i,x}$	0.6283	mrad/Ws
3-phase Q contr. integ. gain	$h^{\text{q}}_{i,3\varphi}$	16.923	1/s
nominal voltage amplitude	V_g	$110\sqrt{2}$	V
nominal frequency	ω	$2\pi 50$	rad/s
inductive impedance	L	2.8	mH

Table II: System parameters.

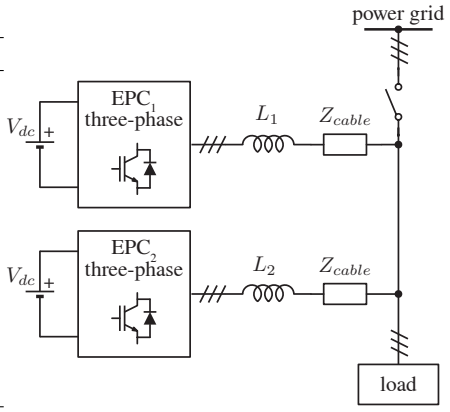

Fig. 6: Structure of the prototype.

The state-space matrices result:

$$A=\begin{bmatrix} -3\gamma_p k_p & 0 & 0 & 0 & k_p & 0 \\ 0 & -\frac{1}{2}h^{\text{p}}_{i,a}\gamma_p & 0 & 0 & 0 & 0 \\ 0 & 0 & -\frac{1}{2}h^{\text{p}}_{i,b}\gamma_p & 0 & 0 & 0 \\ 0 & 0 & 0 & -\frac{1}{2}h^{\text{p}}_{i,c}\gamma_p & 0 & 0 \\ -3h^{\text{p}}_{i,3\varphi}\gamma_p & 0 & 0 & 0 & 0 & 0 \\ 0 & 0 & 0 & 0 & 0 & -h^{\text{q}}_{i,3\varphi}\frac{3\gamma_q k_q}{1+3\gamma_q k_q} \end{bmatrix}$$

$$B=\begin{bmatrix} 0 & 0 & 0 & 0 \\ \frac{2}{3}h^{\text{p}}_{i,a} & -\frac{1}{3}h^{\text{p}}_{i,b} & -\frac{1}{3}h^{\text{p}}_{i,c} & 0 \\ -\frac{1}{3}h^{\text{p}}_{i,a} & \frac{2}{3}h^{\text{p}}_{i,b} & -\frac{1}{3}h^{\text{p}}_{i,c} & 0 \\ -\frac{1}{3}h^{\text{p}}_{i,a} & -\frac{1}{3}h^{\text{p}}_{i,b} & \frac{2}{3}h^{\text{p}}_{i,c} & 0 \\ h^{\text{p}}_{i,3\varphi} & h^{\text{p}}_{i,3\varphi} & h^{\text{p}}_{i,3\varphi} & 0 \\ 0 & 0 & 0 & h^{\text{q}}_{i,3\varphi} \end{bmatrix} \quad C=\begin{bmatrix} \gamma_p & \frac{1}{2}\gamma_p & 0 & 0 & 0 & 0 \\ \gamma_p & 0 & \frac{1}{2}\gamma_p & 0 & 0 & 0 \\ \gamma_p & 0 & 0 & \frac{1}{2}\gamma_p & 0 & 0 \\ 0 & 0 & -\frac{\sqrt{3}}{6}\gamma_p & \frac{\sqrt{3}}{6}\gamma_p & 0 & \frac{\gamma_q k_q}{1+3\gamma_q k_q} \\ 0 & \frac{\sqrt{3}}{6}\gamma_p & 0 & -\frac{\sqrt{3}}{6}\gamma_p & 0 & \frac{\gamma_q k_q}{1+3\gamma_q k_q} \\ 0 & -\frac{\sqrt{3}}{6}\gamma_p & \frac{\sqrt{3}}{6}\gamma_p & 0 & 0 & \frac{\gamma_q k_q}{1+3\gamma_q k_q} \end{bmatrix} \tag{7}$$

while $D=[0]_{6\times 4}$.

State-space representation allows to study system stability through its eigenvalues, and eventually to design the regulators through pole allocation. To this purpose, it is possible to compute in closed-form eigenvalues of matrix A as the roots of $\det[sI-A]$. The characteristic polynomial yields:

$$\psi(s)=\left(s+h^{q}_{i,3\varphi}\frac{3\gamma_q k_q}{1+3\gamma_q k_q}\right)\left(s+\frac{1}{2}\gamma_p h^{\text{p}}_{i,x}\right)^3\left(s^2+3\gamma_p k_p s+3\gamma_p k_p h^{\text{p}}_{i,3\varphi}\right) \tag{8}$$

By (8), controller design can be performed by allocating the eigenvalues of matrix A, on the basis of, for example, time response specifications. The last factor in (8) relates to a complex-conjugate pair of eigenvalues, whose damping factor can be adjusted by control. For example, the critically damped solution (i.e., two coincident real poles) is obtained for $h^{p}_{i,3\varphi}=\frac{3}{4}\gamma_p k_p$, while the damping factor of $\xi=\frac{1}{\sqrt{2}}$ is obtained for $h^{p}_{i,3\varphi}=\frac{3}{2}\gamma_p k_p$. In the following, system parameters in Table II are considered. In this case, $\xi=\frac{1}{\sqrt{2}}$, while the time constants are chosen to be all the same.

Simulations and experimental results

Simulations and experimental tests were performed to validate the control scheme proposed. For experimental tests, the laboratory-scale prototype displayed in Fig. 7 has been employed, implementing the circuit shown in Fig. 6. The controller parameters used are listed in Table II.

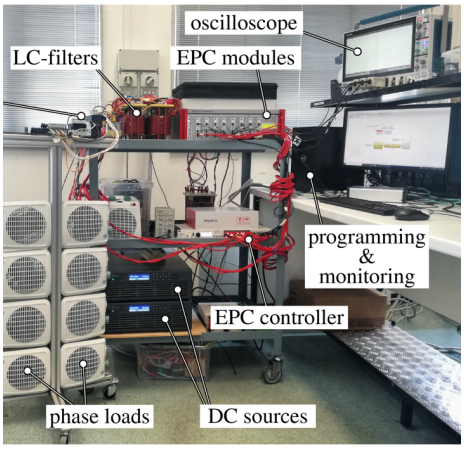

Fig. 7: Laboratory-scale prototype employed in experimental tests.

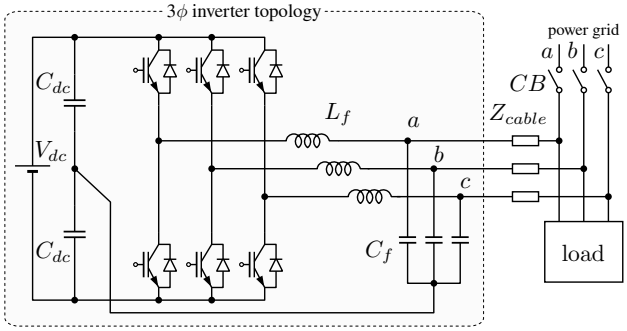

Fig. 8: Three-phase inverter implemented for validation.

Simulation results

Fig. 9 shows the system response of a single EPC to step variations of power references. At $t = 1\,\text{s}$ the first step variation is performed, changing $P_a, P_b, P_c : 0 \rightarrow 500\,\text{W}$. Then at $t = 3\,\text{s}$, $Q_{3\phi} : 0 \rightarrow 1.5\,\text{kW}$. At $t = 5\,\text{s}$ the system is led to unbalanced operating condition by changing $P_c : 500 \rightarrow 750\,\text{W}$. It is possible to see that power reference signals are tracked with zero steady-state error, as expected. Fig. 10 shows the behavior of two different EPCs connected to the grid, both designed according to Table II. A three-phase 10 Ω resistive load is also connected to the grid. Initially, EPC_1 is supplying 1.5 kW active power, while EPC_2 outputs zero active power. Both EPCs supply zero reactive power. At $t = 1\,\text{s}$ the main grid is disconnected: output power regulation is no more possible, thus regulation loops gradually saturate. Between 2 s and 3 s saturation limits are reached, and the controllers smoothly change their operation mode from output power regulation to voltage-forming mode in a droop-like operation.

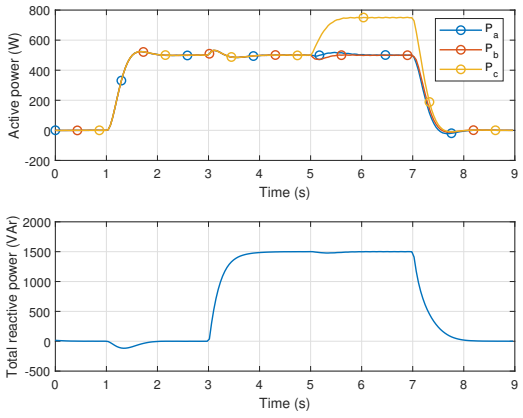

Fig. 9: Step responses of EPC_1 while operating grid-tied.

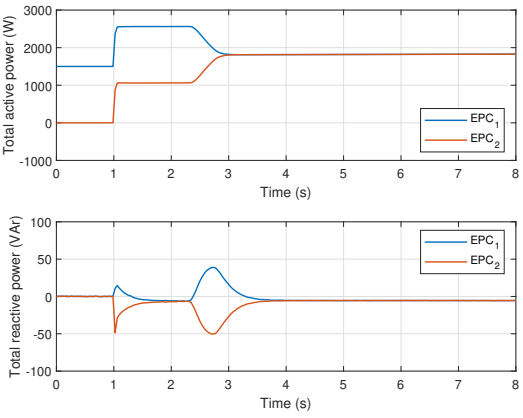

Fig. 10: Grid-connected to islanded transition of EPC_1 and EPC_2 of Fig. 6.

Experimental results

Fig. 11 shows system response to an unbalanced step change of reference signals. In particular, the figure on the left shows output power waveforms P_a, P_b, P_c, and $Q_{3\phi}$, while instantaneous phase voltages and currents are shown on the right. At $t = 0$ the step-change $P_c : 0 \rightarrow 1\,\text{kW}$ is performed. The system correctly tracks the reference signal with zero steady-state error. There is an overshoot visible on P_a and P_b, due to the fact that also total active power is changed. Thus, both synchronization and per-phase

control loops are involved in the regulation. The undershoot in $Q_{3\phi}$ is due to the increase of output active current that causes a voltage drop on the resistive part of the line impedance and leads to an initial reactive power absorption, which is eventually compensated by the controller.

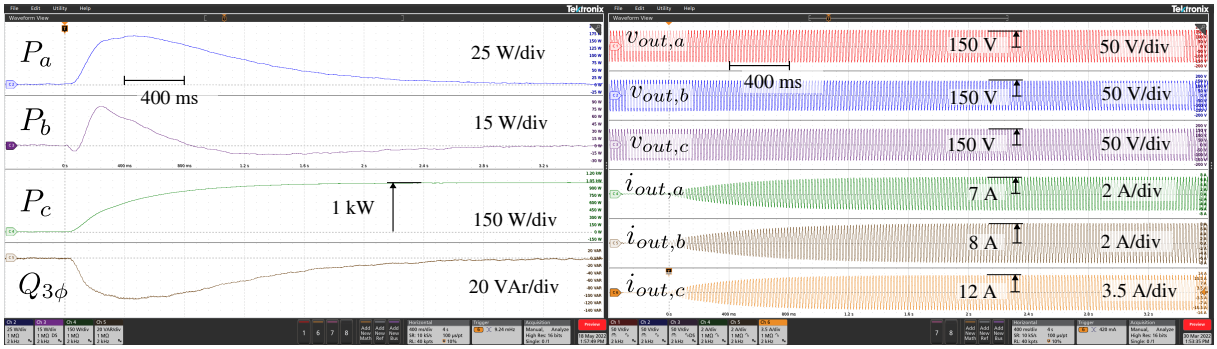

Fig. 11: Unbalanced power reference step-change $P_c : 0 \rightarrow 1\,\text{kW}$ is performed. Output power waveforms are on the left, while instantaneous output voltages and currents are displayed on the right.

Conclusions

A controller achieving per-phase output power regulation in three-phase three-wires systems is proposed herein. In three-phase three-wires systems output active and reactive power can not be independently controlled at each phase: a suitable control scheme is required to perform per-phase output power control with the limited degrees of freedom imposed by the absence of the neutral connection. Together with per-phase output power control, the possibility of island operation is fundamental for uninterrupted power supply in microgrids in case of disconnection from the main grid. The provided experimental validation shown that the proposed controller succeeds in harmoniously integrating phase-by-phase output power tracking and the capability of smoothly transitioning into the islanded operation.

References

[1] S. Chandak and P. K. Rout, "Microgrids During the Outbreak of COVID-19," IEEE Smart Grid Newslett., July 2020.

[2] M. Shahidehpour, M. Yan, P. Shikhar, S. Bahramirad, and A. Paaso, "Blockchain for peer-to-peer transactive energy trading in networked microgrids: Providing an effective and decentralized strategy," *IEEE Electrif. Mag.*, vol. 8, no. 4, pp. 80–90, 2020.

[3] A. S. Vijay, S. Doolla, and M. C. Chandorkar, "Unbalance mitigation strategies in microgrids," *IET Power Electron.*, vol. 13, no. 9, pp. 1687–1710, 2020.

[4] J. M. Guerrero, J. C. Vasquez, J. Matas, L. G. de Vicuna, and M. Castilla, "Hierarchical Control of Droop-Controlled AC and DC Microgrids—A General Approach Toward Standardization," *IEEE Trans. Ind. Electron.*, vol. 58, no. 1, pp. 158–172, 2011.

[5] J. Rocabert, A. Luna, F. Blaabjerg, and P. Rodríguez, "Control of Power Converters in AC Microgrids," *IEEE Trans. Power Electron.*, vol. 27, no. 11, pp. 4734–4749, 2012.

[6] H. Abedini, T. Caldognetto, P. Mattavelli, and P. Tenti, "Real-Time Validation of Power Flow Control Method for Enhanced Operation of Microgrids," *Energies*, vol. 13, no. 22, 2020. [Online]. Available: https://www.mdpi.com/1996-1073/13/22/5959

[7] J. Wang, N. Zhou, Y. Ran, and Q. Wang, "Optimal Operation of Active Distribution Network Involving the Unbalance and Harmonic Compensation of Converter," *IEEE Trans. Smart Grid*, vol. 10, no. 5, pp. 5360–5373, 2019.

[8] F. H. M. Rafi, M. Hossain, M. S. Rahman, and S. Taghizadeh, "An overview of unbalance compensation techniques using power electronic converters for active distribution systems with renewable generation," *Renewable and Sustainable Energy Reviews*, vol. 125, p. 109812, 2020.

[9] P. Tenti and T. Caldognetto, "On Microgrid Evolution to Local Area Energy Network (E-LAN)," *IEEE Trans. Smart Grid*, vol. 10, no. 2, pp. 1567–1576, 2019.

[10] D. I. Brandao, L. S. Araujo, A. M. S. Alonso, G. L. dos Reis, E. V. Liberado, and F. P. Marafão, "Coordinated Control of Distributed Three- and Single-Phase Inverters Connected to Three-Phase Three-Wire Microgrids," *IEEE Trans. Emerg. Sel. Topics Power Electron.*, vol. 8, no. 4, pp. 3861–3877, 2020.

[11] C. Burgos-Mellado, R. Cárdenas, D. Sáez, A. Costabeber, and M. Sumner, "A Control Algorithm Based on the Conservative Power Theory for Cooperative Sharing of Imbalances in Four-Wire Systems," *IEEE Trans. Power Electron.*, vol. 34, no. 6, pp. 5325–5339, 2019.

[12] T. Caldognetto, H. Abedini, and P. Mattavelli, "A Per-Phase Power Controller for Smooth Transitions to Islanded Operation," *IEEE Open Journal of Power Electronics*, vol. 2, pp. 636–646, 2021.

[13] A. Timbus, M. Liserre, R. Teodorescu, P. Rodriguez, and F. Blaabjerg, "Evaluation of Current Controllers for Distributed Power Generation Systems," *IEEE Trans. Power Electron.*, vol. 24, no. 3, pp. 654–664, 2009.

[14] S. Lissandron and P. Mattavelli, "A controller for the smooth transition from grid-connected to autonomous operation mode," in *2014 IEEE Energy Convers. Congr. & Expo.*, 2014, pp. 4298–4305.

[15] K. De Brabandere, B. Bolsens, J. Van den Keybus, A. Woyte, J. Driesen, and R. Belmans, "A Voltage and Frequency Droop Control Method for Parallel Inverters," *IEEE Trans. Power Electron.*, vol. 22, no. 4, pp. 1107–1115, 2007.

[16] W. Yao, M. Chen, J. Matas, J. M. Guerrero, and Z. Qian, "Design and Analysis of the Droop Control Method for Parallel Inverters Considering the Impact of the Complex Impedance on the Power Sharing," *IEEE Trans. Ind. Electron.*, vol. 58, no. 2, pp. 576–588, 2011.